

The metal-insulator transition in amorphous gallium antimonide

S. V. Demishev, Yu. V. Kosichkin, D. G. Lunts, A. G. Lyapin, N. E. Sluchanko, and M. S. Sharambeyan

L. E. Vereshchagin Institute of High-Pressure Physics

(Submitted 20 March 1991)

Zh. Eksp. Teor. Fiz. **100**, 707–724 (August 1991)

We investigate the effect of synthesis conditions on the structure and properties of bulk amorphous gallium antimonide synthesized by the method of quenching under pressure. We show that in the range of pressures $p_{\text{syn}} \approx 90$ kbar the most important parameter for determining the characteristics of a sample is its synthesis temperature, and that when this temperature exceeds a critical value $T_{\text{syn}} \approx 800$ °C, α -GaSb undergoes a metal-insulator transition. On the insulating side of the transition (i.e., for samples made at $T_{\text{syn}} < 800$ °C), the temperature dependence of the specific resistivity $\rho(T)$ shows semiconducting behavior for $T \geq 100$ K with an activation energy $E_a \approx 0.2$ eV, which for $T < 20$ K converts to the Mott law $\ln \rho \propto T^{-1/4}$ for hopping conductivity. On the metallic side of the transition (samples made at $T_{\text{syn}} > 800$ °C) the temperature dependence of the quantity ρ is weak in the range $T \geq 10$ K, while for $T \leq 8$ K a superconductive transition is observed in which the resistance drops smoothly to zero in the interval $1.8 < T < 8$ K. The relative change in electrical conductivity across the metal-insulator transition exceeds a factor of 10^{10} at liquid-helium temperatures. We propose a method for determining the residual fraction X of the crystallographic phase in samples of α -GaSb based on correlation analysis of that part of the x-ray scattering intensity associated with the structure of the material, and find that the order parameter whose change gives rise to the metal-insulator transition in α -GaSb cannot be the magnitude of X . On the basis of analysis of the electrical and magnetic properties of α -GaSb on the metallic side of the metal-insulator transition we determine the parameters for superconductivity in the temperature range $1.8 < T < 630$ K and in the range of magnetic fields $H \leq 150$ kOe, and propose a model in which the anomalies in the characteristics of α -GaSb are associated with the appearance of regions with characteristic dimensions ~ 200 Å in which the composition is nonstoichiometric and short-range order is destroyed.

1. INTRODUCTION

In recent years there has been a marked growth of interest among investigators in semiconducting materials which can be obtained in the amorphous state by methods which employ high pressure for amorphization.^{1–8} On the one hand, this interest stems from the fact that use of such methods solves problems that are “insoluble” by other methods, in particular, the synthesis of amorphous semiconductors from the A^3B^5 group in the form of bulk material.^{3–8} On the other hand, the physical properties of amorphous samples obtained using high pressure exhibit a number of anomalies that are not present in the corresponding amorphous films synthesized by standard methods of thin-film technology. For example, in Refs. 5–7 it was shown that as a result of amorphization under high-pressure conditions gallium antimonide acquires superconducting properties.

However, in the majority of cases the amorphous phases obtained using the methods of Refs. 1–8 turn out to be unstable at room temperature. From the point of view of investigation, the most convenient system of this type known at this time turns out to be α -GaSb, i.e., amorphous gallium antimonide, which is synthesized by quenching at high pressures,^{4–8} and which has a region of stability up to $T = 70$ °C.⁸

Although α -GaSb was first obtained a rather long time ago using a synthesis scheme based on high pressure,³ up to now there has been no systematic investigation of the relationship between synthesis conditions and the structure and properties of α -GaSb. In addition, the nature of the superconductivity observed in α -GaSb,^{5–7} which is not observed

in amorphous gallium antimonide films, remains obscure.

The subject of this paper is the study of the synthesis conditions under which amorphization of gallium antimonide takes place, and the investigation of the relationship between these conditions and the structure of the resulting α -GaSb samples, as well as the electrophysical and galvanomagnetic properties of the latter. Since the appearance of superconductivity in a semiconductor material is a problem of interest in its own right, we will devote special attention to investigating the superconducting properties.

2. EXPERIMENTAL METHOD

Our procedure for synthesizing samples of α -GaSb is shown schematically on the p - T phase diagram of GaSb given in Fig. 1. Originally undoped single crystals of GaSb are cut into slabs of diameter ~ 2.5 mm and thickness ≤ 1.5 mm, and then subjected to the combined action of high pressure p_{syn} and temperature T_{syn} in a “Toroid” chamber.⁹ After being held at $p_{\text{syn}}, T_{\text{syn}}$ for a period of 30–60 sec (Fig. 1, points A_1 – A_n), the samples are quenched at constant pressure to room temperature (Fig. 1, segment A_i – B). Then the pressure is slowly (over a period ~ 600 sec) decreased to atmospheric pressure (Fig. 1, segment B – C).

In view of the highly corrosive nature of GaSb alloys, we were very careful to avoid contaminating the samples during the synthesis process. The best results were obtained by using an isolating container made of NaCl. The absence of foreign impurities was checked by mass-spectrometry methods.

The structural characteristics of the GaSb samples were

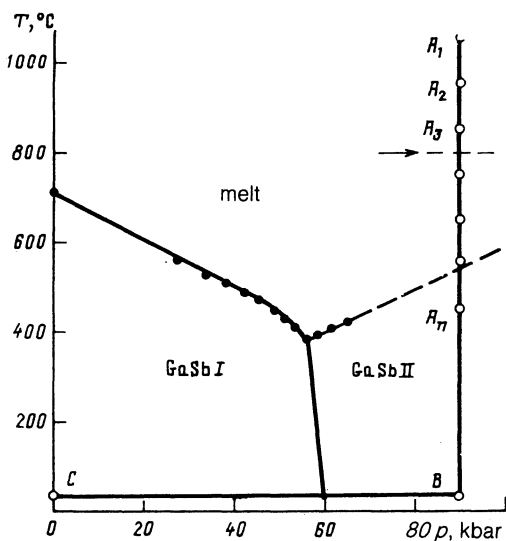


FIG. 1. Phase diagram of GaSb and scheme for synthesis of bulk amorphous samples of gallium antimonide by the method of quenching under pressure. The experimental data on the melting curve under pressure are given in Ref. 24. The arrow denotes $T_{\text{syn}} = 800^\circ\text{C}$. A—melt.

recorded by x-ray methods. The x-ray powder patterns were processed using an automated microdensitometer of our own construction.

For the galvanomagnetic measurements we used the standard method in the temperature interval 1.8–630 K, applying magnetic fields $H < 150$ kOe generated by a Bitter-type magnet (using a "Solenoid" apparatus from the Institute of General Physics, USSR Academy of Sciences). The method of preparing the ohmic contacts to the sample was described in Ref. 5.

3. THE INFLUENCE OF SYNTHESIS CONDITIONS ON THE STRUCTURE OF α -GaSb SAMPLES

The structure and properties of α -GaSb samples obtained using the scheme shown in Fig. 1 is determined by the following parameters: the temperature T_{syn} and pressure p_{syn} , the rate of quenching dT/dt (i.e., the rate of motion along the line A–B in Fig. 1), and the rate of depressurization dp/dt (i.e., the rate of motion along the line B–C in Fig. 1).

The most critical step in the amorphization of GaSb is found to be increasing the pressure p_{syn} above the pressure $p_{\text{tr}} \approx 60$ kbar at which the phase transition GaSb I \rightarrow GaSb II (Fig. 1) occurs, in which the diamond like lattice (GaSb I) is converted into a β -Sn-type lattice (GaSb II); in fact, amorphization is impossible in the range $p_{\text{syn}} < p_{\text{tr}}$. This result coincides with well-known data in the literature regarding amorphization under high pressure.¹⁻³

In the interval $p_{\text{syn}} > 70$ kbar $> p_{\text{tr}}$, this method leads to strong disordering of the structure of the gallium antimonide samples for values of the parameter T_{syn} in the range $400 < T_{\text{syn}} \leq 1400^\circ\text{C}$. Figure 2 shows that portion of the x-ray scattering intensity $I(s)$ associated with crystalline order, obtained by subtracting the incoherent and apparatus-induced components from experimental curves of the optical density of the powder patterns for the samples under discussion. It is clear that quenching under pressure has transformed the sharp crystalline lines that are characteristic of originally single-crystal samples (Fig. 2, curve 1) into broad maxima—the amorphous "halo" (Fig. 2, curves 2, 3).

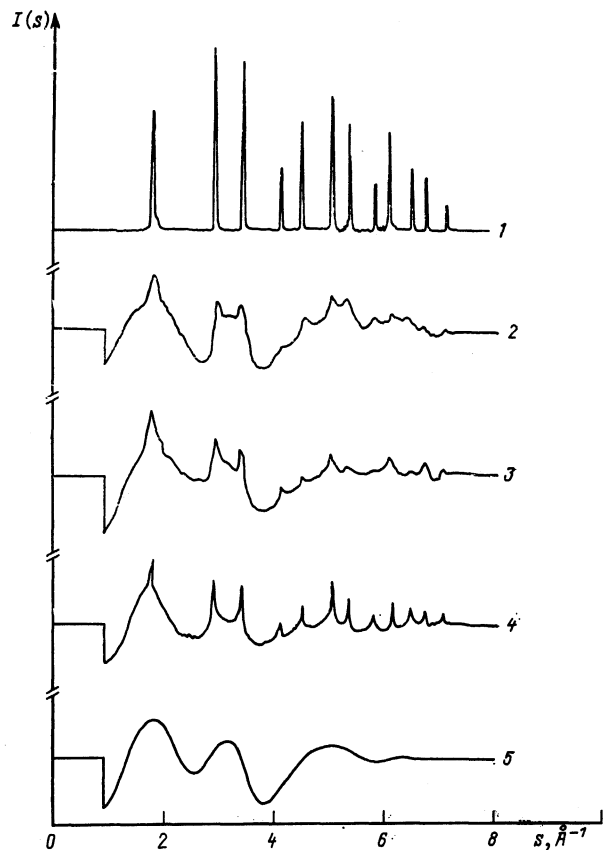


FIG. 2. Structure-related portion of the x-ray scattering intensity for various samples of GaSb: 1—original single crystal; 2—sample of GaSb obtained for $p_{\text{syn}} = 90$ kbar and $T_{\text{syn}} = 670^\circ\text{C}$; 3—sample of α -GaSb obtained for $p_{\text{syn}} = 90$ kbar and $T_{\text{syn}} = 1150^\circ\text{C}$; 4—mixture of amorphous and crystalline phases used as a calibration of the correlation method; 5—reference spectrum for α -GaSb; $s = (4\pi/\lambda) \sin \theta$.

It is noteworthy that varying the rate of quenching in the interval $1-10^3$ K/sec does not significantly change the structure and physical properties of α -GaSb. This fact apparently indicates that the synthesis technique under discussion here differs from standard methods used in the amorphization of alloys by quenching, in which the parameter dT/dt and the critical rates of cooling associated with it play a decisive role.¹⁰

The question of how the rate of depressurization dp/dt affects things is more complicated. Due to limitations that are intrinsic to the method used here, we were not able to vary this parameter over a very wide range. In this work the value of dp/dt was fixed essentially at $dp/dt \approx 0.1$ kbar/sec. We found that the synthesis temperature turned out to be the controlling factor in determining the physical properties of bulk samples of α -GaSb; in view of this, we have focused our attention on the changes in the characteristics of α -GaSb induced by varying T_{syn} in this paper. For this reason, the rate of quenching and the synthesis pressure were kept at the constant values $dT/dt \approx 10^2$ K/sec and $p_{\text{syn}} \approx 90$ kbar. The original positions of the samples of GaSb are shown on the phase diagram (Fig. 1, points A_1-A_n).

Analysis of the data of Fig. 2 showed that even the most disordered samples of GaSb still exhibited crystalline lines characteristic of the original gallium antimonide, although in considerably weakened form (compare curves 1–3 in Fig. 2). In all the samples we studied that were obtained by

quenching under pressure, we found no indications of lines that could be associated either with structural modifications of GaSb or with ordered phases of Ga or Sb. In this situation it is natural to assume that the samples obtained using the scheme of Fig. 1 were in fact a mixture of amorphous and crystalline phases, i.e., $(a\text{-GaSb})_{1-X} \cdot (c\text{-GaSb})_X$.

In order to interpret our results it is vital to have a quantitative determination of the parameter X in the formula $(a\text{-GaSb})_{1-X} \cdot (c\text{-GaSb})_X$. We accomplished this by using a special method based on analysis of the $I(s)$ data (Fig. 2), which we describe below.

To first approximation, the following relation is valid for the structure-related portion of the intensity of x-ray scattering by the mixture $(a\text{-GaSb})_{1-X} \cdot (c\text{-GaSb})_X$:

$$I(s) = A [X\varphi_c(s) + (1-X)\varphi_a(s)], \quad (1)$$

where $\varphi_c(s)$ and $\varphi_a(s)$ are the structure factors¹¹ of the crystalline and amorphous phases respectively, and $s = (4\pi/\lambda) \sin \theta$. For $I(s)$ the following condition holds:

$$\int_0^\infty I(s) ds = 0, \quad (2)$$

which follows from the properties of the functions φ_c and φ_a and expresses the principle of conservation of scattering intensity.¹¹ We define the correlation function $I_1 * I_2 = f(\tau)$ using the formula

$$I_1 * I_2 = \int_0^\infty I_1(s-\tau) I_2(s) ds. \quad (3)$$

Note that in processing the experimental spectra $I(s)$ we replace the upper limit of integration in Eqs. (2) and (3) by $s_{\max} \approx 8 \text{ \AA}^{-1}$ (Fig. 2). Let us also introduce the reference spectra for the crystalline and amorphous samples:

$$I_{c0}(s) = A_1 \varphi_{c0}(s), \quad (4)$$

$$I_{a0}(s) = A_2 \varphi_{a0}(s). \quad (5)$$

In contrast to the reference spectrum I_{c0} , which is known (Fig. 2, curve 1), we have no direct measurement of the function I_{a0} , since all the samples of $a\text{-GaSb}$ we investigated contained some fraction of the crystalline phase. However, because crystalline features were observed in the spectra $I(s)$ of our samples only within narrow intervals of values of the structure argument and were rather small in amplitude, we extracted the reference spectrum for an amorphous sample $I_{a0}(s)$ by averaging the experimental curves $I(s)$ of the most disordered samples and excluding the crystalline features (Fig. 2, curve 5).

The correctness of this procedure for extracting the reference spectrum for the amorphous sample is based on the approximate equality $\varphi_a(s) \approx \varphi_{a0}(s)$, which follows both from direct comparison of curves 2–4 in Fig. 2 and from comparison of parameters which can be determined using the $I(s)$ curve.

For example, the spatial scale for intermediate ordering (medium-range order) L_{MRO} , which can be calculated using the Selyakov formula¹²

$$L_{MRO} = \frac{\lambda}{\Delta\theta \cos \theta_0}, \quad (6)$$

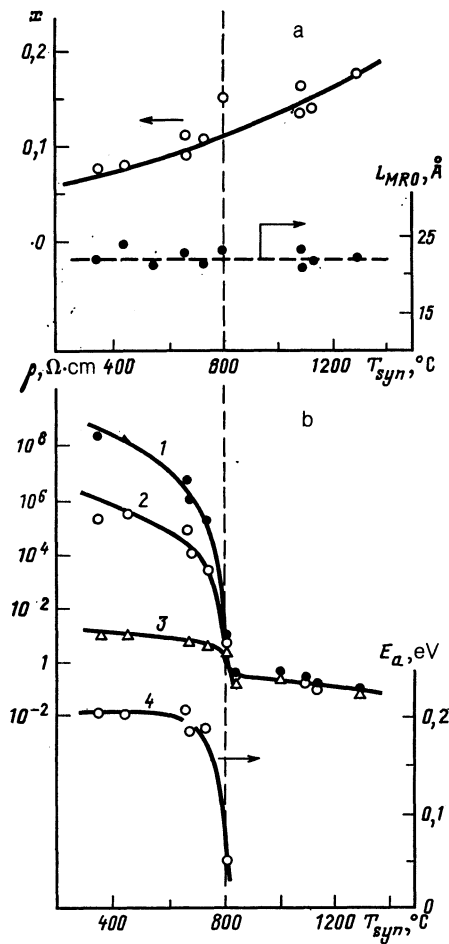


FIG. 3. Changes in the structure (a) and electrophysical properties (b) of $a\text{-GaSb}$; the plots of $\rho(T_{\text{syn}})$ were obtained by varying the synthesis temperature. 1—4.2 K; 2—100 K; 3—300 K; curve 4 is the function $E_a(T_{\text{syn}})$.

is found to depend only weakly on T_{syn} and equals $L_{MRO} \approx 21 \text{ \AA}$ (Fig. 3). In Eq. (6), λ is the wavelength of the x-rays, while $\Delta\theta$ and θ_0 give the width and position of the first amorphous "halo." We note that variations in the shape of the curves $\varphi_a(s)$ from sample to sample can act as a source of uncontrolled error in this method for determining X .

In contrast to the structure factor φ_a of $a\text{-GaSb}$, for the crystalline portion entering into the composition of the mixture $(a\text{-GaSb})_{1-X} \cdot (c\text{-GaSb})_X$ the equality of φ_{c0} and φ_c is destroyed. It is clear from Fig. 2 (curves 2, 3) that the crystalline lines for $(a\text{-GaSb})_{1-X} \cdot (c\text{-GaSb})_X$ are considerably broader than those of a single crystal (curve 1). For a quantitative account of this broadening we use the approximation method given in Ref. 12, with a trial function of Gaussian form, which describes the experimental shape of the curves to within 2%. Then the structure factor φ_c is given by the formula

$$\varphi_c(s) \approx \sum_i \frac{Z_i}{\pi^{1/2} \gamma_i} \exp \left[- \left(\frac{s-s_i}{\gamma_i} \right)^2 \right] + \varphi_0, \quad (7)$$

where the parameters Z_i , γ_i , and s_i specify the corresponding amplitude, width, and position of the i th crystalline line, and φ_0 is chosen from the normalization condition (2). Our analysis of the shape of the crystalline lines in the spectrum

$I(s)$ for the mixtures $(a\text{-GaSb})_{1-X} \cdot (c\text{-GaSb})_X$ showed that the ratio of amplitudes Z_i in the spectrum of the mixture remained the same as in the single crystal (Fig. 2, curve 1), while the half-widths γ_i varied weakly from line to line, and that for calculating the concentration X it was sufficient to set $\gamma_i = \gamma$. In this approximation the structure factors φ_c and φ_{c0} differ only in the values of the parameter γ .

After some elementary transformations of the correlation functions $I_{c0} * I$ and $I_{a0} * I$ which take into account (1)–(5) and (7), we find that

$$Y = \alpha \bar{Y}, \quad \alpha = \frac{A_1}{A_2}, \quad (8)$$

$$\bar{Y} = \frac{(I_{c0} * I_{a0})(I_{a0} * I) - (I_{a0} * I_{a0})(I_{c0} * I)}{(I_{c0} * I_{a0})(I_{c0} * I) - D(I_{a0} * I)}$$

where $Y = X/(1-X)$, and the values of the correlation functions are evaluated at $\tau = 0$. The factor D takes into account the width of the crystalline lines in the mixture:

$$D \approx \frac{1}{\pi^{1/2} \bar{\gamma}} \sum_i \psi_i^2, \quad (9)$$

$$\bar{\gamma} = (\gamma^2 + \gamma_0^2)^{1/2}. \quad (10)$$

Here γ, γ_0 are the widths of the spectral lines of the mixture and the reference spectrum, and $\psi_i = A_1 Z_i$ is the area under the crystalline line labelled i in the reference spectrum I_{c0} . In deriving Eqs. (8) and (9) we made use of the obvious relations $\gamma, \gamma_0 \ll \min |s_i - s_j|, i \neq j$, and $\gamma, \gamma_0 \ll s_{\max}$, and also the approximate equality $\varphi_c * \varphi_a \approx \varphi_{c0} * \varphi_a$ at $\tau = 0$. The latter follows from the fact that the function $\varphi_a(s)$ cannot change significantly over a length $\sim \gamma$.

If the values of the coefficients A_1 and A_2 are known, then Eqs. (8)–(10) allow us to find X from the experimental curves $I(s)$. Note that the use of Eq. (10) is not the only way to calculate the parameter $\bar{\gamma}$; it also can be determined directly from analysis of the shape of the curve $I_{c0} * I = f(\tau)$ which for $\tau \rightarrow 0$ has the asymptotic form $f(\tau) \propto \exp(-\tau^2/\bar{\gamma}^2)$.

When A_1 and A_2 are unknown, we can use the following calibration procedure to calculate α . If we add to a sample with mass M_0 containing a concentration X_0 of the crystalline phase Δm of crystalline material, then processing the curve $I(s)$ for such a combined sample (Fig. 2, curve 4) and using (8)–(10) yields

$$\bar{Y} = \frac{\Delta m}{m_0 \alpha (1 - X_0)} + \frac{X_0}{\alpha (1 - X_0)}. \quad (11)$$

Consequently, by investigating the function $\bar{Y} = f(\Delta m)$, which is a straight line, we can find α and X_0 by using its slope and intercept on the ordinate. It is obvious that the original calibration sample should satisfy the condition $\gamma \approx \gamma_0$.

The procedure described here was used to estimate the error in our determination of X , which for our experiments lay within the range 5–20%. It comes as no surprise that use of the correlation method for processing the spectra $I(s)$ improves the accuracy as a rule over ranges of the crystalline phase concentration that are not too large, i.e., $X \leq 50\%$.

The function $X(T_{\text{syn}})$ obtained in this way is shown in Fig. 3. The amount of crystalline phase increases as a function of the synthesis temperature. It is interesting that the

most amorphous samples of GaSb, i.e., with the smallest X , are obtained for $T_{\text{syn}} \sim 400^\circ\text{C}$, while quenching from a melt ($T_{\text{syn}} \sim 1000^\circ\text{C}$, see Ref. 4) results in increased fractions of the crystalline phase.

It is also noteworthy that in the temperature range $T_{\text{syn}} \sim 1100\text{--}1300^\circ\text{C}$ the quantity X attains a value $X_c \sim 15\text{--}17\%$, which corresponds to the percolation threshold for the crystalline phase [the densities of $a\text{-GaSb}$ and $c\text{-GaSb}$ are the same;⁴ consequently, the mass and volume relative concentrations of the components in the system $(a\text{-GaSb})_{1-X} \cdot (c\text{-GaSb})_X$ coincide].

4. METAL-INSULATOR TRANSITION IN $a\text{-GaSb}$. INSULATING SIDE OF THE TRANSITION

The synthesis temperature almost completely determines the behavior of the electrophysical characteristics of our samples of $a\text{-GaSb}$. Varying T_{syn} in the neighborhood $T_{\text{syn}} \sim 800^\circ\text{C}$ causes large changes in the value of the specific resistivity ρ and the character of its temperature dependence $\rho(T)$ (Fig. 3). The quasimetallic type of conductivity which is characteristic of samples synthesized at high temperatures $T_{\text{syn}} > 800^\circ\text{C}$ changes over to a semiconducting type of conductivity in the temperature range $T_{\text{syn}} < 800^\circ\text{C}$; the relative change in the specific resistivity with synthesis temperature can be ten orders of magnitude when measured at liquid-helium temperatures.

From this we conclude that changing the synthesis temperature T_{syn} induces a metal-insulator transition in $a\text{-GaSb}$.

On the insulating side of the transition ($T_{\text{syn}} < 800^\circ\text{C}$) for $T > 100\text{ K}$ the temperature dependence of the specific resistivity follows an activated law:

$$\rho \propto \exp\left(\frac{E_a}{k_B T}\right). \quad (12)$$

The activation energy remains practically constant, i.e., $E_a \approx 0.2\text{ eV}$, up to $T_{\text{syn}} \sim 750^\circ\text{C}$ and rapidly decreases for $T_{\text{syn}} \sim 800^\circ\text{C}$ (Fig. 3).

In the region of low temperatures ($T \leq 20\text{ K}$) the dependence (12) goes over to a Mott law:

$$\ln \rho \propto \left(\frac{T_0}{T}\right)^{1/4}, \quad (13)$$

which is characteristic of variable-range hopping conductivity (Fig. 4). The parameter T_0 , which determines the slope of those portions of the curve $\rho(T)$ that are linear in the coordinates $\ln \rho = f(T^{-1/4})$, decreases as $T_{\text{syn}} \rightarrow 800^\circ\text{C}$ from a value $T_0 \sim 2.9 \cdot 10^4\text{ K}$ (Fig. 4, curves 1, 2) to $T_0 \sim 230\text{ K}$ (Fig. 4, curve 3).

This character of the temperature dependence of the specific resistivity on the insulating side of the metal-insulator transition agrees very well with what is known about the energy spectrum and current transport in amorphous materials, according to which¹³ bands of localized states are present in the forbidden gap of amorphous semiconductors within which hopping conductivity can take place. In this case, the change in the parameters of the localized states as we approach the metal-insulator transition point is responsible for the change in T_0 .

We note that the quantity E_a obtained in this paper (see Fig. 3) is in good agreement with known data on amorphous

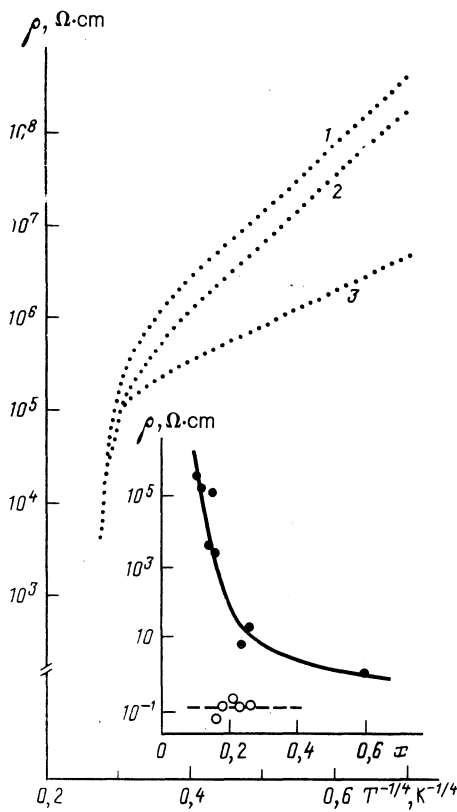


FIG. 4. Hopping conductivity in *a*-GaSb: 1— $T_{\text{syn}} = 350^\circ\text{C}$, 2— 450°C , 3— 670°C . In the inset we show the function $\rho(x)$ for $T = 100\text{ K}$ for two groups of samples: $T_{\text{syn}} < 800^\circ\text{C}$ (the dark dots) and $T_{\text{syn}} > 800^\circ\text{C}$ (the light dots).

films of GaSb synthesized by condensation on a cold substrate,¹⁴ for which the activation energy lies in the range 0.14–0.25 eV. However, the parameter T_0 in the Mott law ranges from $2.8 \cdot 10^8\text{ K}$ to $3.1 \cdot 10^7\text{ K}$ for amorphous films of GaSb, which considerably exceeds the maximum value of T_0 in bulk samples of *a*-GaSb. This difference is apparently due to an increase in the localization by roughly an order of magnitude in samples of *a*-GaSb obtained under high-pressure conditions; however, further investigations are necessary to clarify this question.

Let us consider possible reasons for a metal-insulator transition in the system $(a\text{-GaSb})_{1-x} \cdot (c\text{-GaSb})_x$. According to Ref. 4, the concentration of crystalline phase, which increases with T_{syn} (Fig. 3), could play the role of an order parameter. In this model, when the critical value $X = X_c$ is reached the low-resistivity crystal phase shunts the conductivity of the high-resistivity matrix, causing the metal-insulator transition.

However, our structural analysis data (Fig. 3) imply that values of $X \geq X_c = 0.15\text{--}0.17$ can be achieved only for $T_{\text{syn}} > 1100^\circ\text{C}$, while the metal-insulator transition occurs for $T_{\text{syn}} \sim 800^\circ\text{C}$, i.e., in the range $X < X_c$. Nevertheless, the value $X_c \sim 0.15\text{--}0.17$ is obtained from percolation theory applied to inclusions that are randomly distributed in the sample bulk; for filamentary structures the invariant X_c can be considerably smaller. Therefore we cannot conclude unambiguously that such a two-phase model of $(a\text{-GaSb})_{1-x} \cdot (c\text{-GaSb})_x$ is inapplicable for describing the metal-insulator transition merely by comparing experimental values of X with the theoretical value X_c .

In order to solve this problem experimentally, we investigated samples synthesized at $T < 800^\circ\text{C}$ (the insulating side of the metal-insulator transition) which contained an increased amount of the crystalline phase $X \geq 15\%$ as a result of partial crystallization. In comparing the values of the specific resistivity of these samples with samples on the metallic side of the metal-insulator transition (the inset in Fig. 4; the black dots correspond to $T_{\text{syn}} < 800^\circ\text{C}$, the white dots to $T_{\text{syn}} > 800^\circ\text{C}$), we found that for $T \sim 100\text{ K}$ the quantity $\rho(T_{\text{syn}} < 800^\circ\text{C})$ differed from $\rho(T_{\text{syn}} > 800^\circ\text{C})$ by two orders of magnitude for the same value $X_c \sim 0.2$, and that even after increasing the content of crystalline phase to $X \sim 0.6$ the value of the electrical conductivity of the two different types of samples differed by a factor of 10.

Thus, the appearance of a metal-insulator transition in the $(a\text{-GaSb})_{1-x} \cdot (c\text{-GaSb})_x$ system apparently cannot be explained by a change in the parameter X alone, and in order to clarify the nature of the metal-insulator transition it is necessary to investigate in detail the characteristics of samples on the metallic side of the transition.

5. SUPERCONDUCTIVITY IN AMORPHOUS GALLIUM ANTIMONIDE

Typical functions $\rho(T)$ for samples of *a*-GaSb on the metallic side of the metal-insulator transition ($T_{\text{syn}} > 800^\circ\text{C}$) are shown in Fig. 5 (curve 1). In the region $T \gg 10\text{ K}$ the temperature dependence of the specific resistivity is weak, while for $T \leq 10\text{ K}$ the resistivity decreases smoothly to zero as $T \rightarrow 1.8\text{ K}$. As in samples investigated previously,⁵⁻⁷ the superconducting transition is strongly washed out: an abrupt decrease in ρ begins at $T_m \sim 7\text{ K}$, and the state with $\rho = 0$ is reached for $T < T_p \sim 1.8\text{ K}$ [the value of the residual resistivity is at most $10^{-4}\rho(T = 7\text{ K})$]. The superconduct-

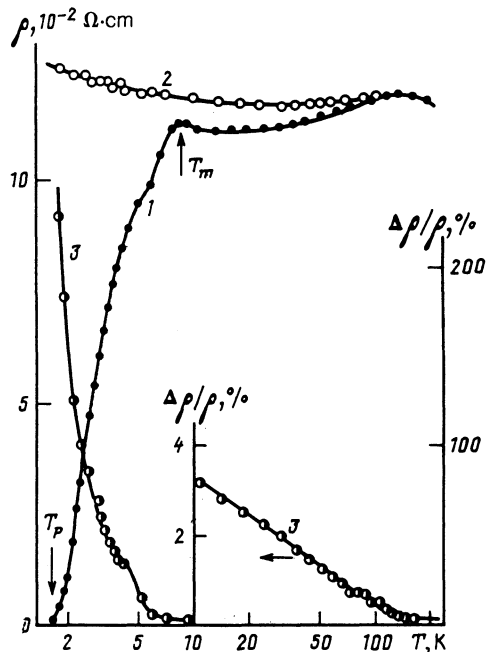


FIG. 5. Temperature dependence of the specific resistivity and magneto-resistivity on the metallic side of the metal-insulator transition ($T_{\text{syn}} = 1100^\circ\text{C}$, sample No. 1): 1— $\rho(T)$ for $H = 0$; 2— $H = 133\text{ kOe}$; 3— $\Delta\rho/\rho$ in a field $H = 133\text{ kOe}$ for a measurement current $i = 5\text{ mA}$. The arrows denote the characteristic temperatures.

ing transition is suppressed by an external magnetic field $H \sim 130$ kOe (Fig. 5, curve 2).

The magnitude of the specific resistivity ρ in the range $T < T_m$ depends strongly on the amplitude of the measurement current i , and ρ vanishes only for currents less than a few tens of microamperes. Increasing the current leads to a considerable increase in the value of ρ . We will investigate the IV characteristics of samples of α -GaSb in more detail below.

It is interesting to note that the sensitivity of the resistivity of α -GaSb samples to magnetic fields is also preserved for $T > T_m$ (see Fig. 5). As the temperature increases from $T \sim 1.8$ K the magnetoresistivity $\Delta\rho/\rho$ (Fig. 5, curve 3) first drops sharply, and then decreases smoothly for $T \gg T_m$ over an extended interval of T (see the inset). For $T \sim 120$ K the curve $\Delta\rho/\rho = f(T)$ has an inflection point, while for $T > 120$ K the magnetoresistivity becomes practically constant. This behavior of $\Delta\rho/\rho$ coincides with data obtained earlier.⁵⁻⁷

Since the superconducting transition in α -GaSb is so spread out and the specific resistivity decreases smoothly to zero, it is reasonable to suppose⁵⁻⁷ that superconductivity in α -GaSb does not appear immediately throughout the volume of the sample, but rather is characterized by a broad spectrum of values of the critical superconducting transition temperature T_c associated with inclusions. Superconductivity first appears in those inclusions with $T_c = T_m$. Further decreasing the temperature results in "scanning" with respect to T_c , as a result of which the fraction of the sample occupied by the superconducting phase $V_s(T)$ increases; once it reaches a critical value $V_s(T_p) = V_p$ at a temperature $T = T_p$, an infinite cluster of superconducting inclusions forms and percolation begins along the superconducting phase, so that $\rho = 0$.

We note that there is no superconductivity on the insulating side of the metal-insulator transition, i.e., this phenomena is a specific characteristic of the metallic side of the transition.

We can offer additional arguments and experimental results to support the present model of superconductivity in α -GaSb. Figure 6 shows the field dependence of the magnetoresistivity corresponding to the region $T \leq T_m$. The initial portion of rapid increase for the curves $\Delta\rho/\rho(H)$ is naturally associated with destruction of superconductivity in regions with $T_c < T_m$. Once the superconductivity is destroyed by a magnetic field, a transition occurs to a smoother linear dependence of the magnetoresistivity (Fig. 6). The presence of some small hysteresis on the curves $\Delta\rho/\rho(H)$ is probably associated with flux pinning, which is characteristic of a type-II superconductor.

Let us define H_m as the field at which the curve $\Delta\rho/\rho(H)$ coincides with its linear asymptotic form. It is obvious that this field corresponds to the maximum critical field H_{c2} that a superconducting inclusion can possess. The function $H_{c2}(T)$ obtained in this way is shown in Fig. 7 (curve 1). We emphasize that in our samples of α -GaSb we observed rather large values of the maximum critical field— $H_{c2}(0) \approx 95$ kOe. It is a characteristic of the curves $\rho(H, T)$ (see Figs. 5 and 6) on the metallic side of the metal-insulator transition that their shape is reproduced from sample to sample, and that the initial transition temperature $T_m \sim 7-8$ K does not depend on T_{syn} .

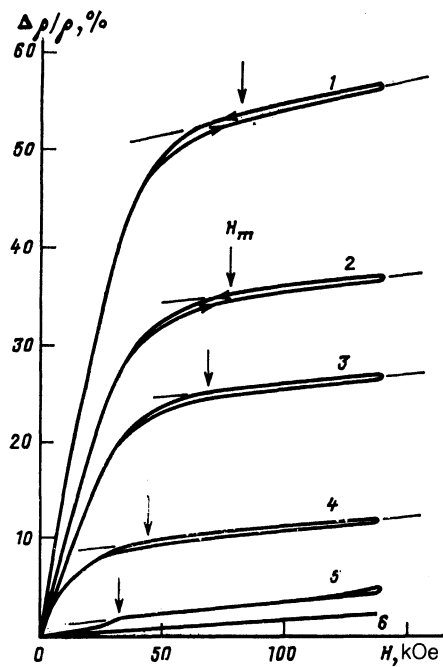


FIG. 6. Magnetoresistance as a function of magnetic field for various temperatures at $i = 5$ mA ($T_{syn} = 1100^\circ\text{C}$, sample No. 1): 1— $T = 2.98$ K; 2—3.6 K; 3—4.2 K; 4—5.2 K; 5—5.8 K; 6—14.3 K. The arrows denote the characteristic magnetic fields H_m .

Measurements of the magnetic properties of α -GaSb samples (Fig. 7, curve 2) in weak magnetic fields ($H \leq 1$ Oe) show that at liquid-helium temperatures the samples are diamagnetic (at room temperature α -GaSb is weakly paramagnetic); however, the value of the magnetic susceptibility χ is only $\sim 10^{-5}$. If we identify $4\pi|\chi|$ with the volume occupied by the superconducting phase, then at the temperature $T_p \sim 1.8$ K for which percolation occurs in the superconducting phase we can estimate $V_s \sim 4\pi|\chi| \sim 1.5 \cdot 10^{-4}$.

The critical volume fraction required for percolation usually comes to $V_p \sim 0.17$; however, in real systems this

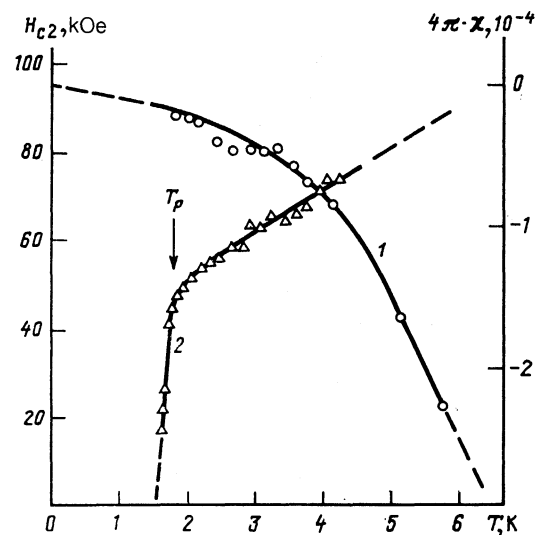


FIG. 7. Characteristic magnetic fields and magnetic susceptibility for α -GaSb: 1— $H_m = H_{c2}(T)$ (sample No. 1); 2— $\chi(T)$ (sample No. 2), $T_{syn} = 1100^\circ\text{C}$.

value can be considerably smaller, e.g., in cases where the inclusions are filamentary in structure. Nevertheless, the quantity $4\pi|\chi|$ is clearly too small for us to explain it as exclusively due to the shape of the inclusions. It is more likely that such a small value of χ in *a*-GaSb is due to the fact that the penetration depth of the magnetic field Λ considerably exceeds the characteristic size a of the superconducting inclusions, i.e., $a \ll \Lambda$. If we use the well-known formula for a spherical superconducting particle of diameter a as an estimate, then the susceptibility of the sample at the percolation limit can be approximated by the expression

$$\chi \approx -V_p \frac{a^2}{10\pi\Lambda^2}. \quad (14)$$

For *a*-GaSb, taking into account $V_p \approx 0.17$, Eq. (14) gives $(a/\Lambda) \sim 5 \cdot 10^{-2}$, and for typical values of $\Lambda \sim (10^{-4} - 10^{-5})$ the characteristic size of the superconducting inclusions comes to $a \sim (500 - 50) \text{ \AA}$.

The temperature dependence of the magnetic susceptibility (Fig. 7, curve 2) has a feature at $T \approx T_p$: the smooth increase of the absolute value of χ as the sample is cooled below $T < T_m$ is replaced by a segment of rapid growth in $|\chi|$ for $T \leq T_p$. This behavior corresponds in a natural way to what is known about the formation of an infinite cluster: at the percolation limit $V_s(T) = V_p$ the density is small, while for $V_s(T) > V_p$ the volume of the infinite cluster increases rapidly; this corresponds to the portion of rapid increase of $\chi(T)$.

A characteristic feature of the superconducting state in *a*-GaSb is the dependence of the specific resistivity, and consequently V_s , on the magnitude of the measurement current i . This behavior for $T < T_m$ can be explained in several ways.

First of all, the characteristics of the contacts between superconducting particles are important. The presence of weak links causes an increase in the current to decrease the average size of the superconducting cluster; furthermore, tunneling through the boundaries between normal and superconducting phases gives rise to nonlinear IV characteristics.¹⁵

Secondly, in the interval $T_p \leq T \leq T_m$ current flows through normal regions as well as through the superconducting regions, causing Joule heating of the sample; because $V_s = V_s(T)$, as the current increases the volume of the superconducting phase decreases.

Thirdly, ordinary current-induced disruption of the superconductivity is possible.

The experimental functions $\rho(i)$ for *a*-GaSb measured at constant current and at various temperatures $T < T_m$ are given in Fig. 8 (curves 1-3). In these plots the IV characteristics of the sample were measured directly at liquid-helium temperatures. It is clear that total disruption of the superconductivity takes place for $i > 0.1$ A, and that ρ increases rapidly with current in the range $10^{-2} - 10^{-1}$ A, while in the region $i < 10^{-2}$ A the specific resistivity decreases smoothly as the measurement current decreases.

In order to distinguish effects due to current-induced heating of the medium we investigated the IV characteristics of *a*-GaSb under pulsed conditions (Fig. 8, curve 4). The parameters of the pulses were chosen so that the average heating of the sample within the time of the pulse $\Delta T \sim i^2 R$ (where R is the resistance of the sample) would be two

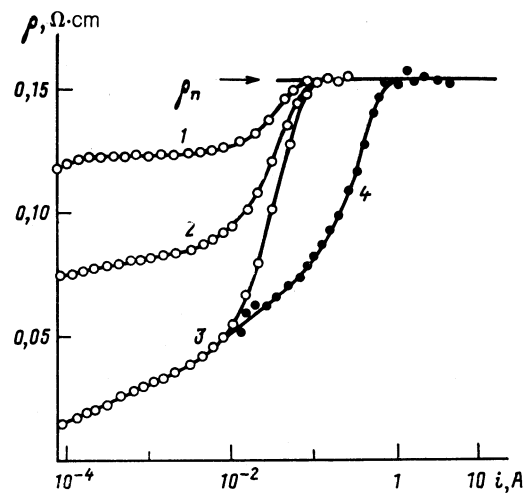


FIG. 8. Destruction of superconductivity by a current in *a*-GaSb. The function $\rho(i)$ is plotted at various temperatures: 1—4.2 K; 2—3.16 K; 3 and 4—2.51 K. Curves 1-3 were measured at constant current, 4 at pulsed current ($T_{syn} = 1100^\circ \text{C}$, sample No. 2)

orders of magnitude smaller than the value obtained from measurement at constant current. A comparison of curves 3 and 4 in Fig. 8, which correspond to $T = 2.5$ K, shows that the Joule heating of the medium begins to be important for currents $i > 10^{-2}$ A. We note that the portion of rapid increase of ρ (Fig. 8, curves 1-4) may be due not only to an increase in the sample temperature but also to current-induced destruction of the superconductivity.

At the same time, the change in ρ in the region $i < 10^{-2}$ A, where thermal effects can be neglected, indicates the presence of weak links that participate in the formation of the percolation superconducting cluster. In this case the observed decrease in ρ with decreasing current is characteristic of Josephson junctions (for the IV characteristics of a tunneling junction, ρ increases rather than decreases at low currents).¹⁵

It should also be noted that the increase of the amplitude of the change in ρ with decreasing temperature in the interval $i \leq 10^{-2}$ A (see Fig. 4, curves 1-3) is in agreement with the percolation picture of the superconducting transition in *a*-GaSb. For Josephson tunneling through normal regions in a percolation chain of inclusions the effective number of breaks in the chain (the number of weak links) will decrease as the temperature decreases; this tendency is most marked for $T \approx T_p$, where even a small change in the infinite-conductivity volume fraction leads to a considerable decrease in ρ .

The presence of weak links in the system of superconducting clusters in *a*-GaSb allows us to make an independent estimate of the characteristic size of the superconducting regions. In Ref. 16, where percolation along a system of superconducting particles connected by weak links was investigated, it was shown that independent of the distribution function for the parameters of the links the size of the particles could be estimated from the relation

$$a \sim \frac{\rho_n}{4R_0 F(T_p)}, \quad (15)$$

where $R_0 = \pi\hbar/4e^2$, ρ_n is the specific resistivity of the sample in the normal state, and $F(T) = (\Delta(T)/T)$

$\cdot \tanh(\Delta(T)/T)$. Here $\Delta(T)$ is the value of the superconductor gap. In the case of *a*-GaSb, which exhibits dispersion of the critical temperatures and values of the gap for the inclusions, it follows from Ref. 16 that Eq. (15) can once again be used as an estimate; however, the value of $F(T)$ in this case should be as large as possible. Substituting into (15) the value $\Delta_m(T_p) \approx 1.76T_m$ for samples with the maximum critical temperature¹⁵ and our data on ρ_n (Fig. 5), we obtain a size estimate of $a_m \sim 240 \text{ \AA}$.

The data we have obtained allow us to estimate the other superconducting parameters of regions with $T_c = T_m$. It follows from Eq. (14) that the maximum contribution to the susceptibility is given by regions with minimum value of Λ , and therefore $\Lambda_m \leq a(V_p/10\pi/\kappa)^{1/2} \sim 4500 \text{ \AA}$. The coherence length ξ_m can be estimated in the standard way:¹⁵

$$\xi_m \sim \left(\frac{\Phi_0}{2\pi H_m} \right)^{1/2} \quad (16)$$

Equation (16) for $T = T_p$ and $H_m = H_{c2}(T_p) \approx 88 \text{ kOe}$ (see Fig. 7) gives $\xi_m \sim 60 \text{ \AA}$, and the Ginzburg-Landau parameter is found to be $\kappa_m \sim \Lambda_m/\xi_m \sim 80$.

These estimates of the parameters for inclusions with $T_c = T_m$ confirm our picture of the superconductivity in amorphous gallium antimonide as type II, with high values of κ .

It is significant that the superconductivity of samples of *a*-GaSb on the metallic side of the metal-insulator transition is metastable (Fig. 9). In samples of *a*-GaSb annealed at $T \sim 150^\circ\text{C}$ over the course of several hours complete crystallization of the amorphous tetrahedral phase occurs.⁸ This effect leads to a considerable decrease in the amplitude of the superconducting transition (Fig. 9, compare curves 1 and 2). However, even after annealing a certain quantity of the superconducting phase continues to be preserved within the bulk of the sample. Complete suppression of superconductivity can be achieved only by raising the annealing temperature to $T \sim 350^\circ\text{C}$, in which case the shape of the curve $\rho(T)$

in the temperature interval $T > T_m$ is practically unchanged (Fig. 9, curve 3).

6. DISCUSSION OF RESULTS

Because superconductivity is a specific feature of samples on the metallic side of the metal-insulator transition, it is natural to search for a connection between the rapid change of the electrophysical characteristics at $T_{\text{syn}} \sim 800^\circ\text{C}$ and the superconducting anomalies. With this goal in mind, we analyzed probable candidate mechanisms for superconductivity in *a*-GaSb starting with the experimental data (Figs. 3–9) including our data on structural analysis (Figs. 2 and 3).

To begin with, we note that the data on the effect of crystallization and annealing on superconductivity in *a*-GaSb show that superconductivity in *a*-GaSb cannot be associated with the tetrahedral amorphous phase, since the superconducting features are preserved after it completely crystallizes. In the previous Refs. 5 and 6 the possibility that crystalline clusters of small size in the mixture $(a\text{-GaSb})_{1-x}(c\text{-GaSb})_x$ might become superconducting through enhancement of the electron-phonon interaction due to the influence of the insulating amorphous neighborhood was considered. However, since residual superconductivity is preserved after annealing at $T \sim 150^\circ\text{C}$, which is accompanied by almost complete crystallization of the *a*-GaSb (Fig. 9, curve 2), this possibility appears rather unlikely; furthermore, the appearance of superconductivity cannot be explained within the framework of the simplest two-phase model which we have used to discuss the data on structural analysis.

At the same time, our x-ray structural analysis data (Fig. 2) allow us to conclude that the samples under discussion are not contaminated by metastable high-pressure crystalline phases of Ga, Sb or GaSb, which are superconducting and which might preserve their superconductivity in locally stressed regions. Under these circumstances, the superconductivity in the samples under study is most likely due to the presence of disordered phases of the system Ga-Sb that differ from the amorphous tetrahedral phase.

If the concentration of these phases is not large, it is much more difficult to detect them using the curves $I(s)$ (Fig. 2). The presence of a noncrystalline phase different from *a*-GaSb gives rise to rather small changes in the shape of the curve $\varphi_a(s)$; the nature of our numerical procedure (see Sec. 3) implies that these changes will ultimately lead to errors in determining X . Using what we know regarding errors in our determination of the value of X , we arrive at a crude estimate of only 3–5% for the concentration of possible uncontrolled inclusions which differ from *a*-GaSb.

One of these phases could be a superconducting metallic glass; however, according to the data of Ref. 17 the maximum temperature T_c of this phase cannot be greater than 4.5 K, which is hard to reconcile with the temperature $T_m \sim 7 \text{ K}$.

Among the metastable superconducting phases of the Ga-Sb system, one of the most promising candidates is amorphous gallium,¹⁸ whose parameters $T_c \approx 8.4 \text{ K}$ and $H_c \approx 100 \text{ kOe}$ are close to the values 7–8 K and $H_m \approx 95 \text{ kOe}$ (Figs. 5 and 7) for *a*-GaSb; however, the resistive transition in amorphous gallium is sharp, unlike the smeared out transition of *a*-GaSb.¹⁸

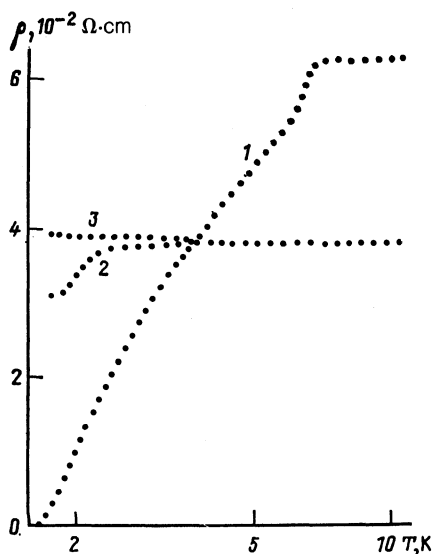


FIG. 9. The effect of annealing on the superconducting transition in *a*-GaSb ($T_{\text{syn}} = 1100^\circ\text{C}$, sample No. 3): 1—original sample, 2—sample after a first anneal (3 hrs, 150°C), 3—sample after a second anneal (30 min, 350°C).

The appearance of superconducting inclusions of amorphous gallium in the bulk of the sample implies local disruption of stoichiometry and of the short-range-order characteristics in the amorphous GaSb network. In general, the composition of such a nonstoichiometric region is expressed by the formula $\text{Ga}_{1-y}\text{Sb}_y$ (where $0 < y < 1$).

In Ref. 19 it was shown that in the range of compositions $y < 0.5$ superconductivity in $\text{Ga}_{1-y}\text{Sb}_y$ arises when the excess concentration of gallium is ~ 55 at%, and T_c varies between 1 K (for 55 at% Ga) and 8.4 K (amorphous gallium). This result allows us to associate the smearing-out of the superconducting transition for α -GaSb with dispersion in the composition of the superconducting cluster $\text{Ga}_{1-y}\text{Sb}_y$.

We note that in addition to regions with excess gallium it is necessary to take into account the possible presence of regions with excess antimony (since the original sample GaSb was stoichiometric in composition; the loss of antimony during synthesis can be neglected). It is known that amorphous antimony is not a superconductor, but is rather a Mott insulator, and for $T \leq 77$ K has a resistivity $\rho_n \approx (20-600) \Omega\text{-cm}$.²⁰ At the same time, there are indications of the existence of metastable noncrystalline phases of Sb which are superconductors with $T_c \sim 6-7$ K, so that in general clusters with the composition $\text{Ga}_{1-y}\text{Sb}_y$ may turn out to be important for both $y < 0.5$ and $y > 0.5$.

The evidence we have presented so far leads us to believe that both superconductivity and the metal-insulator transition in bulk samples of amorphous gallium antimonide are due to inclusions of nonstoichiometric composition which possess metallic conductivity.¹⁹ This in turn results in an additional effect over and above the shunting of the electron conductivity of the more resistive amorphous matrix by the less resistive crystalline phase: the electron conductivity of the samples is affected by the presence of an even less resistive critical subnetwork whose resistivity in the normal state, according to the data of Ref. 19, is bounded above by values $\rho \sim 0.1-0.01 \Omega\text{-cm} < \rho_n$ (see Figs. 5, 8, 9).

In view of the small concentration of these inclusions, we assert that this shunting phase is spatially restricted, i.e., the inclusions take the form of thin filaments or channels. The formation of metallic channels in the bulk of the sample for $T_{\text{syn}} > 800^\circ\text{C}$, which for $T < T_m$ gradually begin to superconduct as the temperature drops, explains both the abrupt character of the metal-insulator transition (Fig. 3) and the existence of two groups of $(\alpha\text{-GaSb})_{1-x}(\text{c-GaSb})_x$ samples with different properties and the same composition X of the crystalline phase (see the inset to Fig. 4). In this case the subnetwork of metallic channels is obviously absent for samples on the insulating side of the metal-insulator transition.

We now propose a model that explains why a subnetwork of metallic channels appears in samples of amorphous gallium antimonide synthesized at $T_{\text{syn}} > 800^\circ\text{C}$, which in turn explains the origin of the metal-insulator transition in α -GaSb. It is known that GaSb melts congruently at atmospheric pressure; however, its components dissociate as the temperature of the melt increases.²² According to the data of Ref. 23, the melting temperature at $p_{\text{syn}} \sim 90$ kbar is estimated to be $T_{\text{melt}} \sim 550^\circ\text{C}$ (Fig. 1), so that $T_{\text{syn}} \sim 800^\circ\text{C}$ corresponds to superheating of the melt. If the character of GaSb melting is preserved under high-pressure conditions,

then quenching of a melt with disrupted short-range order ($T_{\text{syn}} > 800^\circ\text{C}$) could result in the appearance of regions in the bulk of the sample with disrupted stoichiometry. However, confirmation of this assertion requires detailed information on the phase diagram of GaSb in the region $p \sim 90$ kbar, which is not available at this time.

As an additional argument in favor of our model of the metal-insulator transition and superconductivity we can point to the results of Ref. 24, where the authors assumed the presence of antimony inclusions in order to interpret features in the light-scattering (Raman) spectra of samples of α -GaSb obtained by quenching of a melt under high pressure. Nevertheless, the detecting of nonstoichiometric inclusions in α -GaSb and studying their spatial distribution by direct methods is a current and pressing problem, and is an invitation to further investigations.

In conclusion we note that the nature of the high-temperature features of the magnetoresistance (Fig. 1) remains unclear. An estimate of the Lorentz contribution to the magnetoresistance for the experimental values of the Hall mobility $\mu \sim 0.8 \text{ cm}^2/\text{V}\cdot\text{sec}$ and $H \sim 130$ kOe gives a value of $\Delta\rho/\rho \sim 0.5(\mu H)^2 \sim 10^{-7}$, which considerably complicates the interpretation of the effect in terms of the standard picture of transport processes when taken together with the presence of features at $T \sim 120$ K on the curve $\Delta\rho/\rho(T)$. In Refs. 5-7 this feature is associated with the presence of high-temperature superconductivity in α -GaSb; however, we feel that this is a rather unlikely explanation. Nevertheless, a recent paper²⁵ has predicted that a considerable enhancement of superconductivity is possible in samples with fractal structure. Since it is commonly supposed that infinite clusters are fractal in structure, we cannot exclude the possibility that effects of this kind can influence the superconducting properties of amorphous gallium antimonide.

The authors would like to use this occasion to express their heartfelt gratitude to A. A. Abrikosov for discussing a number of aspects of this paper, and also to S. V. Popov and V. V. Brazhkin for their support and help in synthesizing samples of α -GaSb.

¹ E. G. Ponyatovsky, I. T. Belash, and O. I. Barkalov, *J. Non-Cryst. Solids* **117-118**, 679 (1990).

² V. F. Gantmakher, S. E. Esipov, and V. M. Teplinskii, *Zh. Eksp. Teor. Fiz.* **97**, 373 (1990) [*Sov. Phys. JETP* **70**, 211 (1990)].

³ L. B. McWhan, G. W. Hull, and T. R. R. McDonald, *Science* **147**, 1441 (1965).

⁴ M. M. Aleksandrova, S. V. Demishev, Yu. V. Kosichkin, V. I. Larchev, S. V. Popova, and G. G. Skrotskaya, *Pis'ma Zh. Eksp. Teor. Fiz.* **43**, 182 (1986) [*JETP Lett.* **43**, 230 (1986)].

⁵ S. V. Demishev, Yu. V. Kosichkin, A. G. Lyapin, and N. E. Sluchanko, *Pis'ma Zh. Eksp. Teor. Fiz.* **47**, 654 (1988) [*JETP Lett.* **47**, 755 (1988)].

⁶ S. V. Demishev, Yu. V. Kosichkin, A. G. Lyapin, N. E. Sluchanko, and S. E. Chernyak, *Fiz. Tverd. Tela (Leningrad)* **30**, 3691 (1988) [*Sov. Phys. Solid State* **30**, 2119 (1988)].

⁷ S. V. Demishev, Yu. V. Kosichkin, A. G. Lyapin, N. E. Sluchanko, and M. S. Sharambelya, *Abstracts of the Intl. Conf. on Phys. and Engin. of High Pressures*, p. 28. Troitsk, 1989.

⁸ S. V. Demishev, Yu. V. Kosichkin, V. I. Larchev, A. G. Lyapin, S. V. Popova, G. G. Skrotskaya, and N. E. Sluchanko, *Fiz. Tekh. Poluoprovod.* **22**, 1666 (1988) [*Sov. Phys. Semicond.* **22**, 1051 (1988)].

⁹ L. G. Khvostantsev, L. F. Vereshchagin, and A. P. Novikov, *High Temp.-High Press.* **9**, 637 (1977).

¹⁰ S. A. Dembovskii and E. A. Chechetkina, *Glass Formation* [in Russian], p. 27. Moscow, 1990.

¹¹ A. F. Skryshevskii, *Structural analysis of Liquids and Amorphous Solids*, [in Russian], p. 47. Vyssh. shkola, Moscow, 1980.

¹² V. I. Iverova and G. P. Revkevich, *Theory of X Ray Scattering* [in

- Russian], p. 129. Moscow State Univ. Publ., 1978.
- ¹³ N. Mott and E. Davis, *Electronic Processes in Noncrystalline Materials*, Clarendon, Oxford, 1979 (Mir, Moscow, 1982 p. 239.)
- ¹⁴ B. S. Naidu and P. J. Reddy, *Thin Solid Films* **61**, 379 (1979).
- ¹⁵ A. A. Abrikosov, *Fundamentals of the Theory of Metals*, North Holland, Amsterdam, 1988 (Nauka, Moscow, 1987 p. 287.)
- ¹⁶ O. Eutin-Wohlman, A. Kapitulnik, and Y. Shapira, *Phys. Rev. B* **24**, 6464 (1981).
- ¹⁷ M. A. Il'ina, *Fiz. Nizk. Temp.* **13**, 201 (1987) [*Sov. J. Low-Temp. Phys.* **13**, 111, (1987)].
- ¹⁸ B. G. Lazarev, E. E. Semenov, and V. I. Tutov, *Problems in Atomic Science and Engineering. Series on Fundamental and Applied Superconductivity* [in Russian], Vol. 1(4), p. 3 (1976).
- ¹⁹ J. J. Hauser, *Phys. Rev. B* **11**, 738 (1975).
- ²⁰ J. J. Hauser, *Phys. Rev. B* **9**, 2623 (1974).
- ²¹ I. K. Yanson and O. I. Shklyarevskii, *Fiz. Nizk. Temp.* **12**, 899 (1986) [*Sov. J. Low-Temp. Phys.* **12**, 509 (1986)].
- ²² A. R. Regel' and V. M. Glazov, *Physical Properties of Electronic Alloys* [in Russian], p. 102. Nauka, Moscow, 1980.
- ²³ A. Jaraman, W. Klement, and G. C. Kennedy, *Phys. Rev.* **130**, 540 (1963).
- ²⁴ V. N. Denisov, B. N. Mavrin, V. B. Podobedov, and G. G. Skrotskaya, *Pis'ma Zh. Eksp. Teor. Fiz.* **50**, 363 (1989) [*JETP Lett.* **50**, 393 (1989)].
- ²⁵ B. K. Chakrabarti and D. K. Ray, *Solid State Commun.* **68**, 81 (1988).

Translated by Frank J. Crowne